7-1-2012

A Feasibility Study of Time-Lapse Seismic Monitoring of CO_2 Sequestration in a Layered Basalt Reservoir

Murari Khatiwada
University of Oklahoma

Ludmila Adam
Boise State University

Michael Morrison
Boise State University

Kasper van Wijk
Boise State University

A feasibility study of time-lapse seismic monitoring of CO_2 sequestration in a layered basalt reservoir

Murari Khatiwada[1a], Ludmila Adam[b], Michael Morrison[b], Kasper van Wijk[b]

[a] *ConocoPhillips School of Geology and Geophysics, University of Oklahoma*
[b] *Department of Geosciences, Boise State University*

Abstract

We investigate the potential of scattered seismic waves to remotely sense geological sequestration of CO_2 in basalt. Numerical studies in horizontally layered models suggest that strong scattering quickly complicates the wave fields, but also provides a sensitive tool to monitor physical changes in and around the reservoir. These results go hand-in-hand with recent laboratory work and rock-physics modeling that has shown significant changes in the seismic properties of a reservoir undergoing CO_2 sequestration, due to fluid substitution and mineral precipitation.

Keywords: Basalts, wave scattering, CO_2 sequestration, time-lapse monitoring, velocity perturbation

1. Introduction

Storage of carbon dioxide (CO_2) in the subsurface may provide a large-scale option to reduce its emission into the atmosphere. The effectiveness of sequestering CO_2 into deep reservoirs depends on the reservoir storage capacity, stability and risk of leakage (Holloway, 2001; Davis et al., 2003; Torp and Gale, 2004; Rochelle et al., 2004; Benson and Cole, 2008). In basalt, rock-fluid chemical reactions leading to the precipitation of carbonate minerals would reduce the risk of leakage (McGrail et al., 2006; Rogers et al., 2006; Matter et al., 2007; Oelkers et al., 2008; Gislason et al., 2010; Schaef et al., 2010). When this reaction occurs, changes in the elastic properties of basalt will be the combination of fluid substitution of water with CO_2 and carbonate precipitation. Quantifying these elastic changes helps determine the feasibility of remotely monitoring the reservoir with seismic waves.

In addition to the apparently favorable chemical conditions for CO_2 sequestration, flood basalts are also widespread around the world and can potentially host large amounts of CO_2 (McGrail et al., 2006). Figure 1 shows the extent and volume of the Snake River Plain Basalts (SRPB) and the Columbia River Basalts (CRB).

Seismic methods are widely used to remotely monitor changes in reservoir rock properties, and commonly applied in oil and gas reservoir characterization. However, layered basalts pose a considerable challenge to subsurface imaging, mostly due to strong scattering from the sharp impedance contrasts between basalt flows and sedimentary inter-beds (Kumar et al., 2004; Jarchow et al., 1994; Pujol and Smithson, 1991). In this paper we explore how scattered waves in such a high impedance contrast environment can be used to monitor elastic property changes within layers. We model our seismic data based

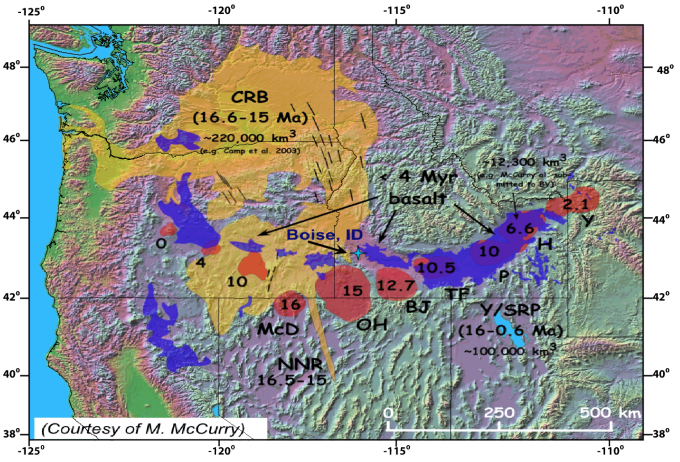

Figure 1: Location and extent of the Snake River Plain (SRP) Basalt, Columbia River Basalt (CRB) and Northern Nevada Rift (NNR) Basalt. The numbers indicate the age of the basalt in millions of years. The sub-groups within the SRP Basalt are defined by time of eruption of the Yellowstone *hotspot*, from older to younger: McDermitt (McD), Owyhee-Humboldt (OH), Bruneau-Jarbidge (BJ), Twin Falls (TF), Picabo (P), Heise (H) and Yellowstone Plateau (Y). The volume of the CRB and the SRP basalt are referenced.

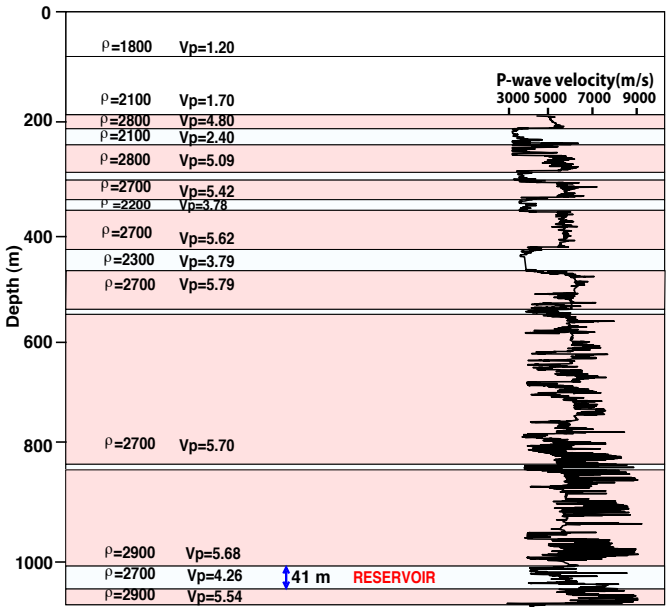

Figure 2: Schematic diagram of multi-layered geological model. Units of density and velocity are in kg/m^3, km/s, respectively. The model parameters are estimated by averaging layers from the sonic log shown.

on the elastic properties of basalt flows with inter-bedded sediments from well logs from CRB at the Hanford site (Washington State, USA, Rohay and Reidel (2005)). The values of velocity and density in each layer are from the blocked sonic and density logs. Figure 2 shows the model with the sonic log overlaid. It is clear that overall the sedimentary interbeds have a significantly lower density and seismic velocities than the basalt flows.

We first explore the anticipated changes in the seismic velocities due to fluid substitution. Second, we present the theory for monitoring velocity perturbations with scattered waves, and finally we model time-lapse seismic on three layered subsurface models, using the predicted velocity changes in the reservoir.

2. Changes in the elastic properties

Changes in the elastic properties of basalts undergoing CO_2 sequestration are a combination of fluid substitution of water with supercritical CO_2, as well as carbonate precipitation. Quantifying these elastic changes remotely with seismic waves will determine the feasibility of effectively monitoring the reservoir. Before we model the wave propagation, we first discuss the anticipated changes in seismic velocities.

2.1. Mineralization

Mineralization of CO_2 into carbonate minerals occurs from the combination of water-carbon dioxide mixtures and divalent metal cations (Ca^{2+}, Mg^{2+}, Fe^{2+}). These cations can be present in low concentrations in formation waters. However, host rocks rich in such metals with high dissolution rates are the target for long-term sequestration and mineralization. Basalt rocks are rich in Ca, Mg and Fe cations and poor in silica, which translates into high dissolution rates of these metals compared to high-silica rocks. The first step for this rock-fluid interaction is that carbonic acid (H_2CO_3) dissociates into bicarbonate (HCO_3^-) and H^+ ions, lowering the pH of the water:

$$\begin{aligned} CO_2 + H_2O &\rightleftharpoons H_2CO_3 \\ H_2CO_3 &\rightleftharpoons HCO_3^- + H^+ \end{aligned} \tag{1}$$

Divalent metal cations in the water precipitate as carbonates:

$$(Ca, Mg, Fe)^{2+} + H_2CO_3 \rightleftharpoons \underbrace{(Ca, Mg, Fe)CO_3}_{\text{carbonate minerals}} + 2H^+ \tag{2}$$

The reaction in equation 2 only occurs if the hydrogen ions are consumed by a different reaction.

The following equations define two of several reactive basalt minerals consuming the free hydrogen and releasing new divalent metal cations into the water (Gislason and Hans, 1987; Matter et al., 2007). These free cations react with the CO_2-water mixture (equation 2) to precipitate as carbonates:

$$\begin{aligned} &\underbrace{Mg_2SiO_4}_{\text{fosterite}} + 4H^+ \rightarrow 2Mg^{2+} + H_2O + SiO_{2(aq)} \\ &\underbrace{CaAl_2Si_2O_8}_{\text{Ca-plagioclase}} + 8H^+ \rightarrow Ca^{2+} + 2Al^{3+} + 4H_2O \\ &+ 2SiO_{2(aq)} \end{aligned} \tag{3}$$

McGrail et al. (2006) and Schaef et al. (2010) report significant carbonate mineralization on crushed samples from the CRB and other basalts around the world. Super-critical CO_2 was mixed with water at 100°C and 10.3 MPa pressure. Carbonate precipitation was observed in as little as 87 days. The rate of mineralization in full rock is unknown, but depends on the available divalent metal cations – which is proportional to the dissolution rate of the minerals – fluid temperature and pressure, solution composition, CO_2 concentration and rock pore surface area. Otheim et al. (2011) show preliminary laboratory velocity measurements on whole basalt cores that have been exposed to a CO_2-water mixture for 15 weeks. They observe an increase in P- and S-wave velocity due to mineral precipitation between 2 and 12%, as well as physical changes on the basalt samples.

2.2. Fluid substitution

When the original fluid in the pore space is replaced or mixed with a different fluid, we call this fluid substitution. For this study, we assume that CO_2 displaces all the formation water in the reservoir. This is likely accurate near the injection hole, but away from the borehole saturation may be patchy. In either case, fluid substitution is the initial effect on the reservoir when CO_2 is injected in a

layered basalt reservoir saturated with formation waters, whereas mineralization would occur later in time. Here we study changes in seismic velocity, when CO_2 fully replaces the formation water in the pore space.

Fluid substitution effects in reservoirs is commonly modeled by Gassmann's equation (Gassmann, 1951):

$$K_{sat} = K_{dry} + \frac{\left(1 - \frac{K_{dry}}{K_{\min}}\right)^2}{\frac{\phi}{K_{fl}} + \frac{1-\phi}{K_{\min}} - \frac{K_{dry}}{K_{\min}^2}}, \qquad (4)$$

which helps us predict the changes in the seismic properties of the saturated rock when one fluid is replaced by a different fluid. In the subsurface, these basalts are saturated with formation water. From velocity and density log data we estimate that the brine-saturated rock has a bulk modulus $K_{sat} = 28.3$ GPa. Assuming a brine with 200,000 ppm of NaCl and at a pressure of 7.6 MPa yields a fluid bulk modulus $K_{fl} = 3.4$ GPa (Batzle and Wang, 1992). The porosity ϕ is estimated at 19% from the density log and the mineral composition of the CRB. The mineral bulk modulus is an average of the bulk modulus of minerals based on XRD information of a CRB sample from Schaef et al. (2010). This particular sample composition has 45.3% olivine, 35.3% plagioclase, 18.3% pyroxene (augite) and 1.0% magnetite. The effective $K_{min} = 91.1$ GPa is obtained from the Voigt-Reuss-Hill bulk modulus average of the forming minerals. With these estimates, equation 4 results in a dry rock bulk modulus $K_{dry} = 17.66$ GPa.

The potential CO_2 reservoir is at 1 km in depth, where the CO_2 is in supercritical (sc) condition: it compresses as a gas, but has the density of a liquid. Sc-CO_2 at 60°C and a pressure of 7.6 MPa has a density of 170 Kg/m^3 and a bulk modulus of 0.01 GPa. The only parameter in equation 4 that changes from a water to CO_2 saturated rock is K_{fl}. From this equation and the properties of sc-CO_2 the estimate for the bulk modulus of the rock fully-saturated with CO_2 is 17.70 GPa. The change from dry to CO_2 saturated rock is small because of the high compressibility of the CO_2. However, in the subsurface we are replacing water by CO_2, so that the bulk modulus of the rock would change from 28.3 GPa to 17.7 GPa, a decrease of 37%. The rock bulk density would also decrease as CO_2 substitutes water. The shear modulus of the saturated rock is expected to remain constant, because fluids have a shear modulus of zero.

The result of this modeling implies that the P- and S-wave velocities change from 4260 m/s to 3886 m/s and 2400 m/s to 2472 m/s, respectively. This means that the P-wave velocity decreases 10% and that the shear velocity increases 3% as CO_2 replaces water. The fluid effect on the shear wave velocity only responds to a density effect. In CRB however, the water salinity at 1 km depth can be as low as 10,000 ppm of NaCl (McGrail et al., 2010). For this brine, the fluid bulk modulus is 2.4 GPa at 7.6 MPa and 60°C. A lower fluid compressibility because of lower salinity increases the estimated dry bulk modulus of the rock. After estimating K_{sat} by Gassmann's relation the predicted CO_2-saturated basalt P-wave velocity is 4062 m/s. This velocity represents a 5% decrease in the P-wave velocity from water to CO_2 saturation. The S-wave velocity would increase by 3%. Two different brines were modeled with Gassmann's equation because continental basalts would probably be saturated with lower salinity brine than basalts erupted in the sea. The modulus calculations for these brines were performed assuming the formation water will be completely substituted by CO_2 and that Gassmann's equation is the theory describing the changes in compressibility of these basalts.

In the field, however, complete brine displacement by CO_2 is probably not widespread. The effect of fluid saturation on velocity from a uniform water-CO_2 mixture is shown in Figure 3. To estimate these velocities for saturated basalts, the fluid-mixture bulk modulus was averaged using the Reuss average, and the fluid density was averaged using an arithmetic mean. Figure 3 shows that if the fluids are uniformly distributed, CO_2 has the largest effect on the P-wave velocity when it represents 6% or less of the total mixture, dropping the velocity from 4260 m/s to 3800 m/s. This type of fluid mixture modeling is applicable for patchy saturation where a patch-size is smaller than a specific length at which wave-induced pore pressures have enough time to equilibrate (Mavko and Mukerji, 1998). However, saturation due to large patches can be modeled in detail with field specific parameters (Kazemeini et al., 2010). For these models, patchy saturation effects on velocity are significantly more sensitive to the water-CO_2 mixture than for a uniform distribution. The purpose of this paper is not to model the effect of partial saturation on seismic velocity, but to show the potential of monitoring changes in velocities by studying the coda waves of seismic signal. To understand the fluid saturation and distribution effect on seismic signatures, future laboratory core measurements and field modeling need to be integrated with the method presented here.

Finally, laboratory experiments by Otheim et al. (2011) conducted on basalt samples from SRPB show that the P-wave velocity decreases between 5 and 10% when CO_2 fully replaces distilled water. Although Gassmann modeling and laboratory measurements on these basalts show a decrease in the P-wave velocity of up to 10%, a more conservative P-wave velocity change of 5% is modeled in this study. If coda wave interferometry turns out to be able to detect a 5% decrease in velocity, this technique would also be applicable to a velocity change of greater value.

2.3. Combined fluid substitution and mineralization effects on elastic properties

Using the basic concepts of physics of materials (Gassmann's theory and rock stiffening after mineralization), we qualitatively predict changes in P- and S-wave velocities. Figure 4 illustrates the P- and S-wave velocity changes as a function of time. In the fluid substitution phase, the P-wave velocity significantly decreases as predicted by Gas-

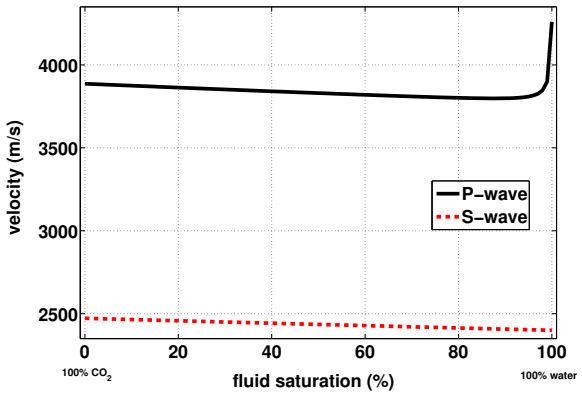

Figure 3: P- and S-wave velocities modeled using a uniform CO_2-water mixture and reservoir parameters. The bulk modulus of the fluid mixture is estimated from the Reuss average. For this fluid distribution model the velocity change is the greatest when CO_2 makes up to 6% of the fluid mixture.

mann's relation but as soon as mineralization occurs, it is possible that the P-wave velocity will increase. For S-waves, the velocity increase during the fluid substitution phase is negligible. For the mineralization phase, however, the S-wave velocity may increase significantly. It is clear from Figure 4 that there is a specific time where fluid substitution and mineralization effects on the P-wave velocity offset each other, and time-lapse data may not show changes in the reservoir in that time window. Laboratory work is in progress to help clarify the trade-off effect on velocity between fluids and mineralization.

3. Coda wave interferometry

Later times in the seismogram (the seismic coda) represent the scattering of seismic waves. These waves often sample the medium well and are thus sensitive to small velocity perturbations. *The active doublet method* (Poupinet et al., 1984; Roberts et al., 1992) and *coda wave interferometry* (CWI) (Snieder, 2006) seek to find the relation between travel time perturbation and velocity changes in the medium.

The travel time for a wave in a medium with velocity v is

$$t = \int_P \frac{1}{v} ds, \tag{5}$$

along the path P. The perturbed travel time due to a small velocity perturbation Δv is

$$t + \Delta t = \int_P \frac{1}{v + \Delta v} ds \approx \int_P \left(\frac{1}{v} - \frac{\Delta v}{v^2} \right) ds, \tag{6}$$

based on a first order Taylor expansion. Solving equations 5 and 6, we find that

$$\int_P \frac{1}{v} ds + \Delta t = \int_P \frac{1}{v} ds - \int_P \left(\frac{\Delta v}{v^2} \right) ds, \tag{7}$$

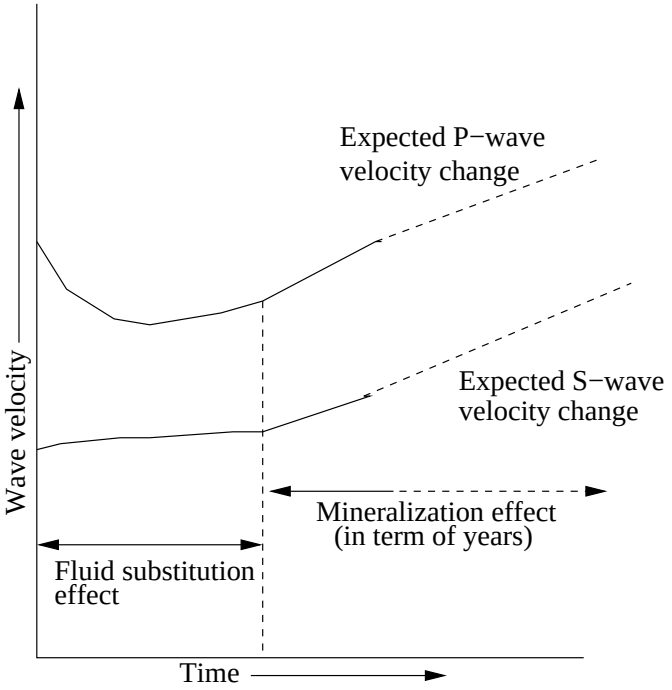

Figure 4: A conceptual diagram showing the effect of CO_2 injection on P- and S-wave velocity due to fluid substitution and mineralization.

$$\Delta t = -\left(\frac{\Delta v}{v} \right) \int_P \frac{1}{v} ds = -\left(\frac{\Delta v}{v} \right) t, \tag{8}$$

assuming the velocity perturbation is constant in space. This result can be rewritten as

$$\frac{\Delta t}{t} = -\frac{\Delta v}{v}. \tag{9}$$

This means that for a given velocity change in the entire medium, the change in travel time is equal but of opposite sign.

4. Numerical modeling of seismic wave propagation

Based on the previous calculations, we apply coda wave interferometry to models with a conservative estimate of the decrease in the P-wave speed of 5% in a reservoir after CO_2 sequestration. We perform wave propagation simulations with the Spectral Element Method (SEM, Komatitsch et al., 2002) in layered media. While the source is a point source spreading in two dimensions, we only consider receivers on the (vertical) line perpendicular to the horizontal layering. The sides of the model in this example are sufficiently far away so that no side-reflected energy re-enters the recordings in the borehole. Top and bottom of the model, however, are reflecting boundaries. The central frequency of the source is 60 Hz and we generally use 40 receivers 20 m apart in the borehole.

Layered basalt is well known for its strong multiple scattering attenuation, but intrinsic attenuation can also

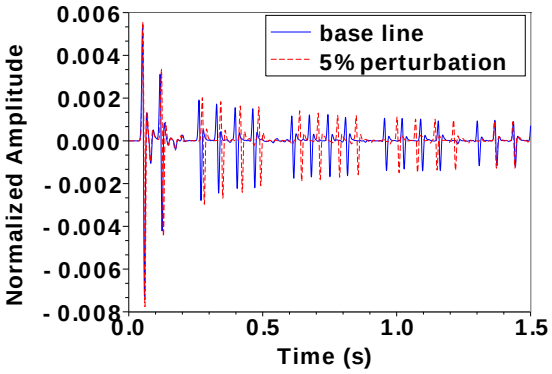

Figure 5: Waveforms before and after a 5% velocity perturbation across the entire homogeneous model. The reflections from top and bottom of the model show a lag time. This lag time increases, as time increases.

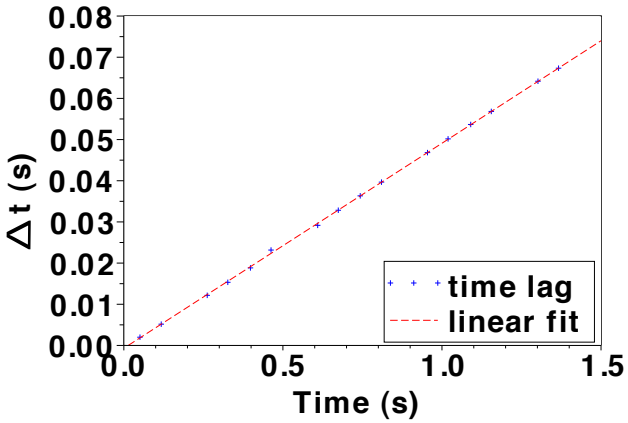

Figure 6: Time lags Δt between coherent reflections as a function of travel time t between the pre- and post-injection wavefields displayed in Figure 5. The slope provides an accurate estimate of the relative velocity decrease of 5%.

attenuate seismic waves in basalt. Pujol and Smithson (1991) studied the seismic wave attenuation properties of the CRB and based on their findings, we adopt a global value for the intrinsic attenuation of P-waves equal to $Q_p = 40$.

4.1. A homogeneous model

In a homogeneous acoustic model with dimension of $x = 9000$ m by $z = 1000$ m and velocity $v = 5250$ m/s, we simulate wave propagation from a point source at 400 m depth from the surface. We simulate 2D wave propagation before and after a global change in the velocity of $\Delta v = -5\%$, where the signals recorded are the direct arrival and the reflections from top and bottom of the model. The waveforms for the receiver at 270-m depth are shown in Figure 5. From the difference between the pre- and post-perturbation waveforms and equation 9, we find that $\frac{\Delta t}{t} = 4.98 \pm 0.04\%$ (Figure 6). This value corresponds to the actual change in velocity $\frac{\Delta v}{v}$ = -5%.

Layer (m)	Velocity (m/s)	Density (kg/m^3)
0-1000	5800	2700
1000-1041	4260	2300
1041-1060	5540	2700

Table 1: Numerical modeling parameters for the three-layer model.

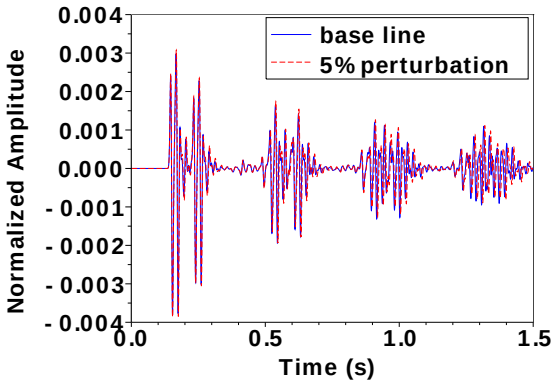

Figure 7: Waveforms in a three-layer model from a source in the reservoir and a receiver above it.

4.2. A three-layer model

Next we consider a three-layer model, where the parameters are listed in Table 1. Similarly, we reduce the velocity in the reservoir layer by 5%, and compare the pre- and post-injection seismic data for a source in the reservoir and a receiver 10 m above it (Figure 7). As is evident from the complexity of the waveforms, even with only three layers, there are many possible travel paths from source to receiver.

Figure 8 shows the slope of the best-fitting line through the travel-time change as a function of time, for each receiver with the source in the reservoir. Receivers closer to the reservoir are more sensitive to the reservoir change than receivers farther away, but all receivers underestimate the velocity change in the reservoir according to equation 9. The same observations were made for VSP measurements in Zhou et al. (2010). The reason for the underestimation is that each travel path from source to receiver has spent only a fraction of its travel time in the perturbed reservoir. Zhou et al. (2010) used detailed knowledge of the subsurface velocities to model the expected coda-wave changes. Next, we analytically solve the changes for a three-layered model, for the situation with the highest sensitivity: with source and receiver in the injection layer. However, sensitivity may be high enough in reality that monitoring can be done down-hole *near* the reservoir, instead of inside. Figure 8 shows a sensitivity that is largest inside the reservoir, decaying away from the reservoir. The ability to use receivers away from the reservoir will depend on the signal to noise ratio of the data. For a detailed investigation of different data acquisition

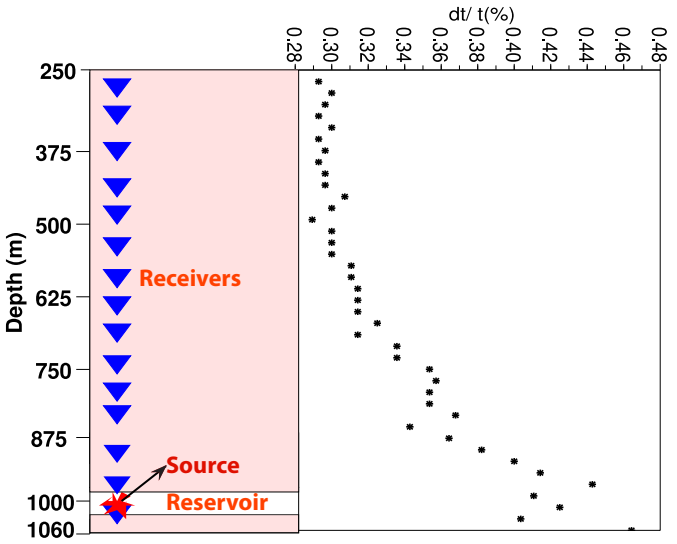

Figure 8: The velocity of a thin reservoir is perturbed by 5%. The travel time difference Δt between corresponding events are estimated for each receiver, as a function of time t. The black symbols represent the best fitting slope of $\frac{\Delta t}{t}$ for each receiver.

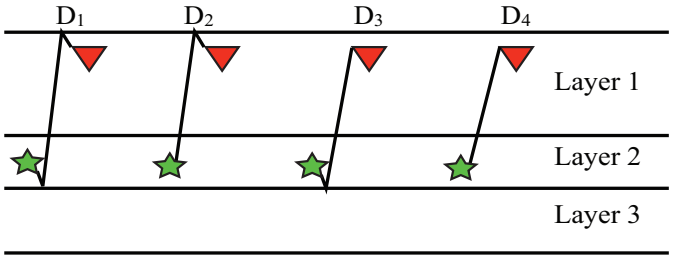

Figure 9: A ray can depart the source up or down and arrive at a receiver from above or below. Source and receiver are in the vertical plane, but are drawn with a horizontal offset to illustrate the ray paths.

geometries for monitoring purposes, we refer the reader to Khatiwada (2009).

In this three-layer model with a localized velocity perturbation, the recorded signal spends a significant time traveling through unperturbed material, and equation 9 must be adjusted to account for this. For random media, Pacheco and Snieder (2006) and Pacheco and Snieder (2005) consider probabilities of time lags due to localized changes for singly and multiply scattered waves. Here, we aim for a deterministic solution:

$$\frac{\Delta v}{v} = \frac{C\Delta t}{t}, \tag{10}$$

where C is a multiplier determined from the relative residence time t_{res} within the perturbed reservoir material:

$$C = \frac{t}{t_{res}}. \tag{11}$$

This multiplier is a function of the medium properties, as well as the location of source and receiver.

Figure 7 shows four separate wave groups, corresponding to the number of times the signal traversed the top layer. Within each wave group are four distinct wave packets, each corresponding to a different number of bounces in the reservoir and/or the four different source/receiver types depicted in Figure 9. Hence, the resident time and thus the value of C varies with time.

All paths in Figure 10 depart the source in the same direction (upward) and arrive at the receiver in the same direction (downward). In addition, the number of multiples in each layer is the same. Even though each path traverses the medium in a different order, their travel time and residence times are the same. We call these paths part of the same cohort. This means their C is constant.

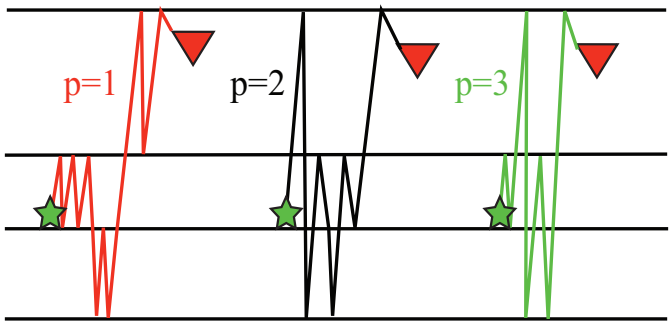

Figure 10: Three different paths with the same total travel time and residence time in the middle layer. Source and receiver are in the vertical plane, but are drawn with a horizontal offset to illustrate the ray paths.

Pre (s)	Post (s)	$\Delta t/t$ (%)	C	$\Delta v/v$(%)
0.9445	0.9475	0.317	15.27	-4.84
0.2890	0.2919	1.003	4.83	-4.85
0.6809	0.6845	0.529	8.40	-4.45
1.4221	1.4274	0.373	12.84	-4.79

Table 2: Results obtained for a three-layer model, with C determined from equation 11.

The travel time for a cohort can be computed as follows:

$$t = t_{type} + 2\sum_{i=1}^{l} n_i \frac{h_i}{v_i}, \tag{12}$$

where t_{type} is the travel time associated with a particular Source/Receiver path, and h_i and v_i are the thickness and velocity of layer i, respectively. The number of multiple pathways in layer i is n_i. The residence time in the reservoir (layer 2 in this case) is

$$t_{res} = \frac{2n_2h_2}{v_2} + t_d, \tag{13}$$

where t_d is the reservoir residence time associated with Source type. Substituting the results of Equations 12 and 13 into Equation 11, results in the C values of Table 2. The average estimate of the velocity perturbation is -4.73%.

4.2.1. Arrivals with different residence times

Equation 11 suffices when travel times and residence times of the individual ray paths can be identified. If rays with differing residence time in the reservoir arrive at a receiver at the same time, we propose:

$$\frac{\Delta v}{v} = \frac{C'\Delta t}{t}, \tag{14}$$

where

$$C' = \frac{\sum_i |A_i| C_i}{\sum_i |A_i|}. \tag{15}$$

A_i is the amplitude of the i-th ray with the same arrival time t, where the amplitude of the ray is:

$$A_i = L_p D_d (R_{12}R_{23})^{n_2} \left[\frac{T_{21}T_{12}R_{10}}{R_{21}}\right]^{s_1} \times (R_{10}R_{12})^{n_1-s_1} \left[\frac{T_{23}T_{32}R_{30}}{R_{23}}\right]^{s_3} (R_{30}R_{32})^{n_3-s_3}. \tag{16}$$

Exponents n_j and s_j are, respectively, the number of layer j multiples and crossings. Apart from those crossings associated with Source/Receiver type (Figure 9), crossings occur in pairs (one coming in, one going out).

Attenuation coefficients (D_d) associated with each Source Receiver Type are defined in Table 3, where T_{ij} and R_{ij} are, respectively, transmission and reflection coefficients associated with a signal moving from layer i into layer j. L_p is a path length factor:

1	D_1	$R_{23}T_{21}R_{10}$
2	D_2	$T_{21}R_{10}$
3	D_3	$R_{23}T_{21}$
4	D_4	T_{21}

Table 3: Source/receiver attenuation coefficients for wave types 1-4.

Start (s)	$\Delta t/t$ (%)	C'	$\Delta v/v$ (%)	$\sigma_{\Delta t}$
0.130	0.231	17.44	-4.02	0.15
0.150	0.533	5.20	-2.77	0.41
0.240	0.167	10.29	-1.72	0.50
0.480	0.125	22.01	-2.75	0.19
0.500	0.240	18.72	-4.49	0.10
0.640	0.438	10.90	-4.77	0.01
0.840	0.143	25.29	-3.62	0.30
0.880	0.341	17.78	-6.06	0.09
1.320	0.311	22.12	-6.87	0.23
1.350	0.281	18.15	-5.10	0.00

Table 4: Estimates of the velocity change in the reservoir of a three-layer model, using Equation 14. Lag times Δt were obtained from crosscorrelating a time window of 40 ms.

$$L_p = \frac{1}{(h_d + 2\sum h_i n_i)^m}, \tag{17}$$

where h_d is the path length associated with Source/Receiver type d defined in Table 3, and the exponent m depends on model geometry. For a two-dimensional model, $m = \frac{1}{2}$.

Even though we managed to track individual rays in the three-layered model, we next extract average values for Δt over time windows of 0.04 s from the lag time of the maximum correlation coefficient. For more complicated models, this more automatic way is likely the method of choice. Per time window, more than one cohort contributes to Δt. C' is determined using Equation 15, and the resulting reservoir changes summarized in Table 4 show that estimates of the reservoir velocity changes are particularly close to the true value when the variance in C' is small.

4.3. A 17-layer model

Finally, we consider a 17-layer model that more accurately represents the geology of a possible CO_2 injection site in the Columbia River Valley, Washington, with thick layers of flood basalt and inter-layered sediments (Figure 2). We numerically compute waveforms from a point source at the injection depth of 1010 m from the surface, before and after a 5% decrease in P-wave velocity in the reservoir.

Based on the observed maximum sensitivity near the reservoir in the three-layered model, we analyze the case where both source and receiver are inside the reservoir. Averaged over $t = 1.5$ s, $\Delta t/t = -\Delta v/v = 0.50 \pm 0.40\%$ (Figure 11). This is not in agreement with the velocity

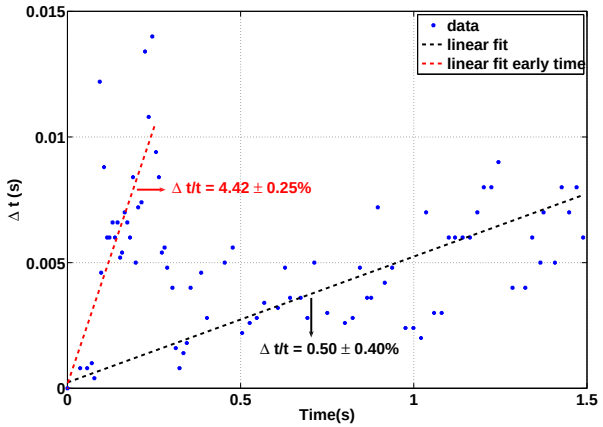

Figure 11: Travel time change analysis due to 5% decrease in velocity for source and receiver both in the reservoir; the black line shows the travel time change for the entire record. The red line indicates the travel time change for early times only.

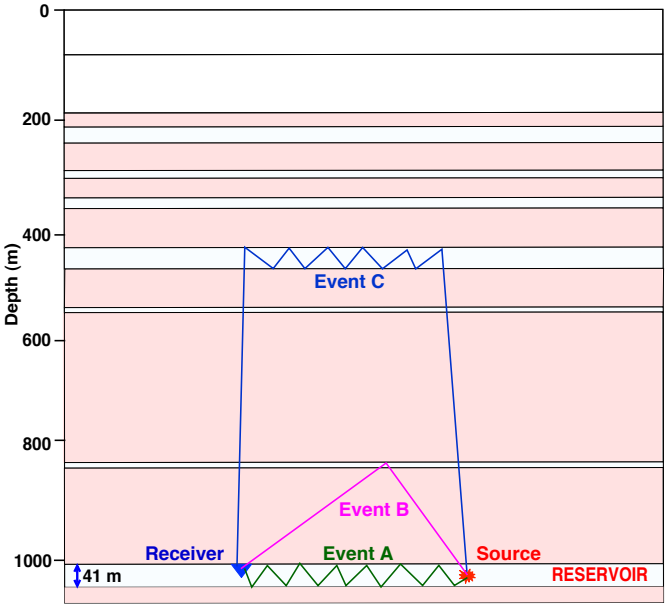

Figure 12: Schematic diagram of some representative wavepaths for both source and receiver in the reservoir.

decrease in the reservoir of 5%. Instead of the rather involved process of determining the residence time versus the total travel time of individual ray paths, we take a more practical view: waves excited in the reservoir are at first mostly trapped because of the relatively high impedance contrast with the massive basalt flows on top and bottom.

We find that in the first $t = 0.25$ s after the source is set off, waves traverse the reservoir up to 12 times. In that time, $\Delta t/t = \Delta v/v = 4.42 \pm 0.25$, based on the regression denoted by the red line in Figure 11. The improvement of the estimate of the velocity perturbation is illustrated in Figure 12, where for early times waves are mostly trapped in the reservoir (event A). At later times, waves that leak out the reservoir can re-enter. Such events see only a small portion of the changes imposed by travel in the reservoir. Thus at later times the recorded signal is dominated by events such as event B and C. Knowledge of the reservoir thickness and medium velocity can aid in estimating the best time window for analyzing velocity changes with coda wave interferometry.

5. Conclusions

Predicting changes in the P- and S-wave velocity for a CO_2 sequestration scenario in basalt rocks is studied with a simple rock physics model. The P-wave velocity decreases up to 10% from fully-water to fully-CO_2 saturated basalts, as estimated from modeling and laboratory data. A conservative estimate of the reservoir velocity change of 5% went into a monitoring study based on coda wave interferometry. Remotely monitoring such small changes in thin reservoirs deep in the earth continues to be a challenge for geophysicists. We present a numerical study of a monitoring technique based on down-hole seismic profiling. We show that coda waves in layered earth models are sensitive to small velocity perturbations, and recovering those changes can be achieved by understanding the propagation of scattered waves within layers. Future work will focus on more realistic earth models and the reality of noisy data.

6. Acknowledgments

We thank the Department of Energy, the Big Sky Carbon Sequestration Partnership, the Center for Advanced Energy Studies and Schlumberger for providing financial support for this research. Also, we thank Dimitri Komatitsch for providing us with the spectral element code and suggestions regarding its use, and Roel Snieder for his many constructive suggestions. We would like to thank Christopher Juhlin, Charlotte Sullivan, and Klaus Holliger for their revisions and reccomendations on improving this manuscript.

References

Batzle, M., Wang, Z., 1992. Seismic properties of pore fluids. Geophysics 11, 1396–1408.

Benson, S. M., Cole, D. R., 2008. CO_2 sequestration in deep sedimentary formations. Elements 4, 325–331.

Davis, T. L., Terrell, M. J., Benson, R. D., Cardona, R., Kendall, R. R., Winarsky, R., 2003. Multicomponent seismic characterization and monitoring of the CO_2 flood at Weyburn Field, Saskatchewan. The Leading Edge 22 (7), 696–697.
URL http://link.aip.org/link/?LEE/22/696/1

Gassmann, F., 1951. Über die elastizität poröser medien. Vierteljahrsschrift der Naturforschenden Gesellschaft in Zürich 96, 1–23.

Gislason, S. R., Hans, P., 1987. Meteoric water-basalt interactions. I: A laboratory study. Geochimica et Cosmochimica Acta 51 (10), 2827–2840.

Gislason, S. R., Wolff-Boenisch, D., Stefansson, A., Oelkers, E. H., Gunnlaugsson, E., Sigurdardottir, H., Sigfusson, B., Broecker, W. S., Matter, J. M., Stute, M., Axelsson, G., Fridriksson, T., 2010. Mineral sequestration of carbon dioxide in basalt: A preinjection overview of the CarbFix project. International Journal of Greenhouse Gas Control 4 (3), 537–545.

Holloway, S., 2001. Storage of fossil fuel-derived carbon dioxide beneath the surface of the earth. Annual Review of Energy and the Environment 26, 145–166.

Jarchow, C. M., Catching, R. D., Lutter, W. J., 1994. Large-explosive source, wide-recording aperture, seismic profiling on the Columbia Plateau, Washington. Geophysics 59 (2), 259–271.

Kazemeini, S. H., Juhlin, C., Fomel, S., 2010. Monitoring CO_2 response on surface seismic data; a rock physics and seismic modeling feasibility study at the CO_2 sequestration site, Ketzin, Germany. Journal of Applied Geophysics 71 (4), 109–124.

Khatiwada, M., 2009. Numerical modeling of time-lapse seismic experiments to monitor CO_2 sequestration in a layered basalt reservoir. Master's thesis, Boise State University.

Komatitsch, D., Ritsema, J., Tromp, J., 2002. The spectral-element method, Beowulf computing, and global seismology. Science 298, 1737–1742.

Kumar, D., Bastia, R., Guha, D., 2004. Prospect hunting below deccan basalt: imaging challenges and solutions. First Break 22, 35–39.

Matter, J. M., Takahashi, T., Goldberg, D., 2007. Experimental evaluation of in situ CO_2-water-rock reactions during CO_2 injection in basaltic rocks: Implications for geological CO_2 sequestration. Geochemistry Geophysics Geosystems 8 (2).

Mavko, G., Mukerji, T., 1998. Bounds on lowfrequency seismic velocities in partially saturated rocks. Geophysics 63 (3), 918–924.
URL http://link.aip.org/link/?GPYSA7/63/918/1

McGrail, B. P., Freeman, C. J., Beeman, G. H., Sullivan, E. C., Wurstner, S. K., Brown, C. F., Garber, R. D., Tobin, D., Steffensen, E. J., Reddy, S., Gilmartin, J. P., 2010. Capture and sequestration of CO_2 at the Boise White paper mill. Tech. rep., Battelle Pacific Northwest Division.

McGrail, B. P., Schaef, H. T., Ho, A. M., Chien, Y.-J., Dooley, J. J., Davidson, C. L., 2006. Potential for carbon dioxide sequestration in flood basalt. Journal of Geophysical Research 111 (B12), B12201.

Oelkers, E. H., Gislason, S. R., Matter, J., 2008. Mineral carbonation of CO_2. Elements 4 (5), 333–337.

Otheim, T. L., Adam, L., van Wijk, K., Batzle, M. L., McLing, T., Podgorney, R., 2011. Co_2 sequestration in basalt: Carbonate mineralization and fluid substitution. The Leading Edge 30 (12), 1354–1359.
URL http://link.aip.org/link/?LEE/30/1354/1

Pacheco, C., Snieder, R., 2005. Localizing time-lapse changes with multiply scattered waves. J. Acoust. Soc. Am. 118, 1300–1310.

Pacheco, C., Snieder, R., 2006. Time-lapse traveltime change of singly scattered acoustic waves. Geophysical Journal International 165 (2), 485–500.
URL http://dx.doi.org/10.1111/j.1365-246X.2006.02856.x

Poupinet, G., Ellsworth, W., Frechet, J., 1984. Monitoring velocity variations in the crust using earthquake doublets - an application to the Calaveris fault, California. Journal Geophysical Research 89, 5719–5731.

Pujol, J., Smithson, S., September 1991. Seismic wave attenuation in volcanic rocks from VSP experiments. Geophysics 56 (9), 1441–1455.

Roberts, P. M., Phillips, W. S., Fehler, M. C., 1992. Development of the active doublet method for measuring small velocity and attenuation changes in solids. Journal of the Acoustical Society of America 91, 3291–3302.

Rochelle, C. A., Czernichowski-Lauriol, I., Milodowski, A. E., 2004. The impact of chemical reactions on CO_2 storage in geological formations: a brief review. Geological Society of London, Special Publications 233, 87–106.

Rogers, K. L., Neuhoff, P. S., Pedersen, A. K., Bird, D. K., 2006. CO_2 metasomatism in a basalt-hosted petroleum reservoir, Nuussuaq, West Greenland. Lithos 92 (1-2), 55 – 82, magmatism and Tectonism of Greenland Rifts - A Tribute to C. Kent Brooks, Four decades of geological research in the Tertiary igneous province of east Greenland, held in honour of C. Kent Brooks.

Rohay, A. C., Reidel, S. P., 2005. Site-specific seismic site response model for the waste treatment plant, Hanford, Washington. Tech. rep., Pacific Northwest National Laboratory.

Schaef, H. T., McGrail, B. P., Owen, A. T., 2010. Carbonate mineralization of volcanic province basalts. International Journal of Greenhouse Gas Control 4 (2), 249–261.

Snieder, R., 2006. The theory of coda wave interferometry. Pure and Applied Geophysics 163, 455473.

Torp, T. A., Gale, J., 2004. Demonstrating storage of CO_2 in geological reservoirs: The Sleipner and SACS projects. Energy 29 (9-10), 1361 – 1369, 6th International Conference on Greenhouse Gas Control Technologies.

Zhou, R., Huang, L., Rutledge, J., Fehler, M., Daley, T. M., Majer, E. L., 2010. Coda-wave interferometry analysis of time-lapse VSP data for monitoring geological carbon sequestration. International Journal of Greenhouse Gas Control 4, 679–686, doi:10.1016/j.ijggc.2010.01.010.